Geochemistry Geophysics Geosystems G3

Article
Volume 13, Number 10
20 October 2012
Q10016, doi:10.1029/2012GC004357
ISSN: 1525-2027

Published by AGU and the Geochemical Society

New constraints on the provenance of the ANDRILL AND-2A succession (western Ross Sea, Antarctica) from apatite triple dating

Massimiliano Zattin and Benedetta Andreucci
Department of Geosciences, University of Padova, Via G. Gradenigo 6, IT-35131 Padova, Italy (massimiliano.zattin@unipd.it; benedetta.andreucci@studenti.unipd.it)

Stuart N. Thomson and Peter W. Reiners
Department of Geosciences, University of Arizona, Tucson, Arizona 85721, USA (thomson@email.arizona.edu; reiners@email.arizona.edu)

Franco M. Talarico
Department of Earth Sciences, University of Siena, Via Laterina 8, IT-53100 Siena, Italy (talarico@unisi.it)

[1] Apatite triple dating (fission track, U-Pb and U-Th/He techniques) has been applied to detrital grains from the sedimentary core drilled during the ANDRILL 2A project, which documents the Miocene history of the Victoria Land Basin (western Ross Sea). High-temperature cooling ages show two main clusters (about 30 and 500 Ma) whereas most of low-temperature data are late Oligocene-Early Miocene in age. These latter data are related to the exhumation of the Transantarctic Mountains south of the Discovery Accommodation Zone. Comparison between low-temperature ages suggests that the Transantarctic Mountains have been in a phase of post-orogenic decay since at least 30 Ma. The Oligocene U-Pb data demonstrate the presence of a volcanic event well before the McMurdo volcanic group, whose onset is commonly places at 19 Ma. The location of the volcanic centers is unknown, but they could be below the Ross Ice Shelf south of drilling site. As a whole, these data indicate a major flow of sediments from south to north with only minor contributions from nearby outlet glaciers of the East Antarctic Ice Sheet.

Components: 14,800 words, 5 figures, 3 tables.

Keywords: (U-Th)/He dating; Andrill; Antarctica; U-Pb dating; apatite triple dating; fission-track dating.

Index Terms: 1140 Geochronology: Thermochronology; 1165 Geochronology: Sedimentary geochronology; 5462 Planetary Sciences: Solid Surface Planets: Polar regions.

Received 23 July 2012; **Revised** 24 September 2012; **Accepted** 24 September 2012; **Published** 20 October 2012.

Zattin, M., B. Andreucci, S. N. Thomson, P. W. Reiners, and F. M. Talarico (2012), New constraints on the provenance of the ANDRILL AND-2A succession (western Ross Sea, Antarctica) from apatite triple dating, *Geochem. Geophys. Geosyst.*, *13*, Q10016, doi:10.1029/2012GC004357.

©2012. American Geophysical Union. All Rights Reserved.

1. Introduction

[2] The influence of Antarctic ice sheets on the global climate system during the Cenozoic has been intensely investigated in the last years, especially after the successful offshore drilling projects in the western Ross Sea [*Hambrey et al.*, 2002; *Barrett et al.*, 2009]. This area is crucial for a better understanding of the ice dynamics as it records the evolution of both East and West Antarctic Ice Sheets, whose variations are a direct response to climatic changes. However, although numerical modeling is able to give some inferences on the mass balance of the ice sheets [e.g., *Pollard and DeConto*, 2009], the role of the Western Ice Sheets (WAIS) during the Miocene is unclear in comparison to that of the East Antarctic Ice Sheet (EAIS), large parts of which have been more or less stable and cold for the last 14 Ma [*Sugden et al.*, 1993; *Sugden and Denton*, 2004].

[3] The recent ANDRILL McMurdo Ice Shelf (AND-1B) project [*Naish et al.*, 2009] and the Southern McMurdo Sound (AND-2A) project [*Harwood et al.*, 2009] had the primary aim to provide a nearly continuous stratigraphic record of the last ca. 20 Ma. The drill sites are located in the southern McMurdo Sound, where the depositional system is influenced by the EAIS outlet glaciers to the west and by the WAIS to the south. The AND-1B 1285-m-long core was recovered from beneath the northwestern corner of the Ross Ice Shelf and allowed the identification of about 58 sequences of advance and retreat of the grounded ice margin during the last 13 Ma [*Naish et al.*, 2008]. The AND-2A 1138-m-long core greatly improved documentation across the warm mid-Miocene climatic optimum and the following cooling, interpreted as major cause of formation of quasi-permanent ice sheet in East Antarctica [*Haywood et al.*, 2009].The recovered succession spans from early Miocene to Pleistocene, with an expanded record in the interval 20–14.2 Ma and a more fragmentary record of the interval 14.2–0 Ma [*Acton et al.*, 2008; *Di Vincenzo et al.*, 2010].

[4] Detrital geochronology and thermochronology allows inferences to be made about the location, age, and exhumation history of source terrains. Because such data are sensitive to variations in the ice-flow patterns, they provide valuable information for the reconstruction of ice sheet dynamics over time. A first paper by *Zattin et al.* [2010], based on apatite fission track (AFT) dating on sediments from the AND-2A core, suggested the existence of a previously undetected Oligocene/Early Miocene exhumation phase in the region between the Blue-Koettlitz and Skelton-Mulock glaciers (Figure 1), therefore pointing out the importance of fluctuation of local glaciers in the Royal Society Range and/or ice sheet expansions into the McMurdo Sound mainly sourced by larger outlet glaciers located further south. This idea is consistent with provenance studies of gravel-size clasts carried out by *Sandroni and Talarico* [2011] and *Talarico and Sandroni* [2011], as well as by heavy mineral signatures detected by *Hauptvogel and Passchier* [2012] and by petrographical and mineralogical characteristics of Ca-amphibole–bearing metamorphic clasts [*Talarico et al.*, 2011]. In this paper, we augment the AFT data set with more samples mostly from the uppermost 285 m of the AND 2-A core and additionally present the first U-Pb and (U-Th)/He data on apatites from the AND 2-A core. Combination of these different techniques, as it covers a large temperature window (ca. 500–60°C), can reveal both the crystallization and exhumation age of a grain, thus providing detailed information about source region. In more detail, we can also distinguish fast-cooled apatites derived from an Oligocene volcanic event from others related to bedrock exhumation. As a whole, these data confirm a provenance from southern regions and provide new constraints on the reconstruction of ice paleo-flows.

2. Geological Setting

[5] The AND-2A drill site is located in the southern part of the McMurdo Sound (77°45.488′S; 165°16.613′E), near the termination of the Koettlitz and Blue glaciers (Figure 1). The drilled succession is composed of sediments deposited in the southern margin of the Victoria Land Basin (VLB), a structural half-graben that forms part of the Western Antarctic Rift system, whose activity started probably in the Cretaceous [*Cooper and Davey*, 1985]. Regional seismic reflection surveys show that the drilled succession is composed of a series of clinoform sets that can be subdivided into four discrete main phases of basin-forming activity: 1) Early Rift (34–29 Ma), 2) Main Rift (29–24 Ma), 3) Passive Thermal Subsidence (24–13 Ma), and 4) Renewed Rifting (Terror Rift: 13 Ma to present) [*Fielding et al.*, 2006; *Henrys et al.*, 2007; *Fielding et al.*, 2008]. The western border of the VLB is delimited by the Transantarctic Mountains (TAM), a 4-km high mountain range acting as a barrier to the direct flowing of the EAIS into the Ross Sea.

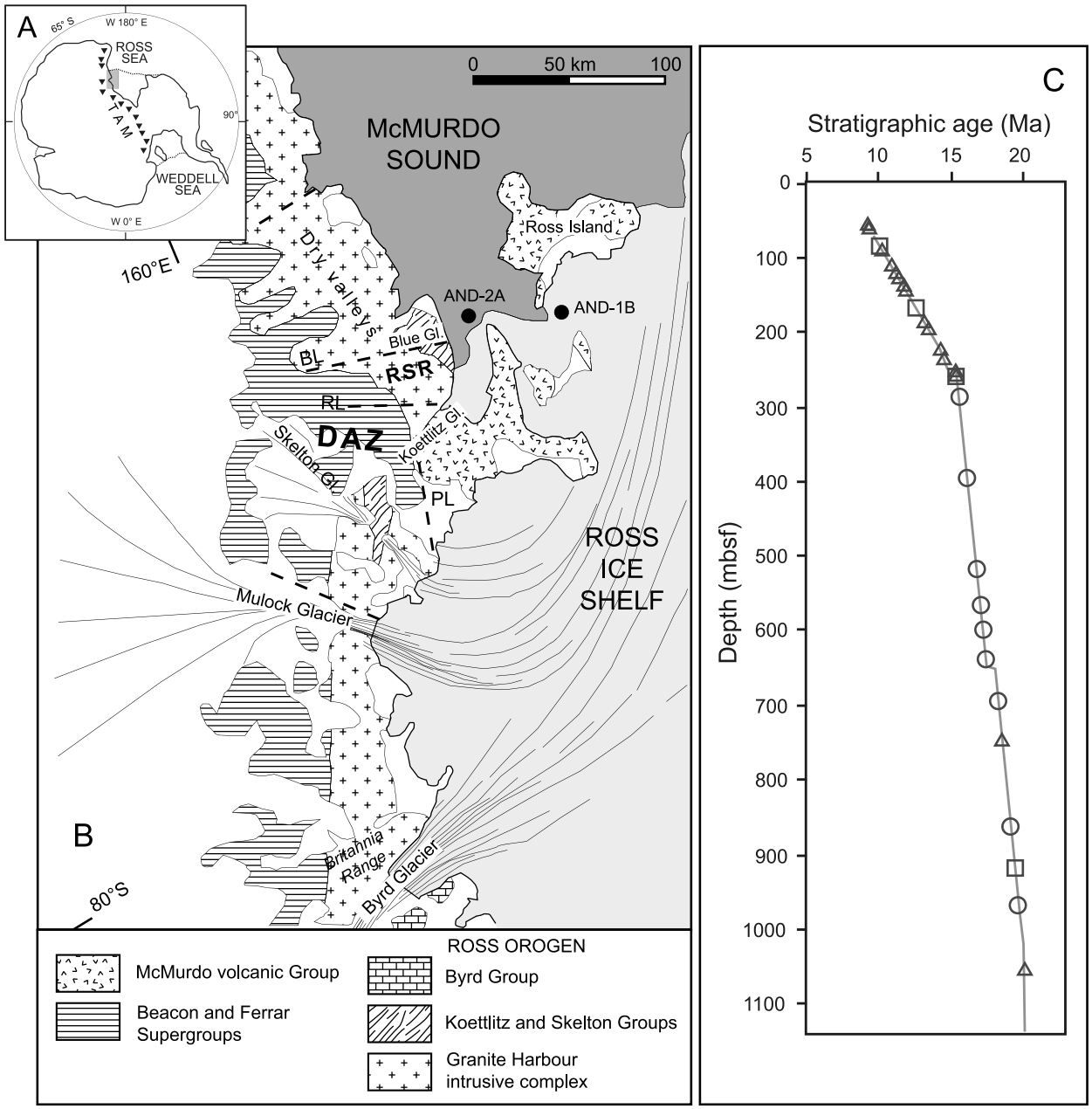

Figure 1. (a) The Antarctic continent and location of Figure 1b (gray box). (b) Geological map [after *Talarico et al.*, 2011] with location of ANDRILL drill holes AND-1B and AND-2A. Present-day glacial flow lines are after *Fahnestock et al.* [2000]. RSR: Royal Society Range. DAZ: Discovery Accommodation Zone. Dotted lines represents main tectonic lineaments. BL: Blue Lineament; RL: Radian Lineament; PL: Pyramid Lineament. (c) Age model for AND-2A [*Di Vincenzo et al.*, 2010] with samples for AFT analysis (triangles), AFT and U-Pb analysis (circle), triple dating (square).

[6] The TAM are composed of late Proterozoic-Cambrian metamorphic rocks (Koettlitz and Skelton Groups [*Gunn and Warren*, 1962; *Findlay et al.*, 1984; *Cook and Craw*, 2002]) intruded by Cambrian-Ordovician granitoids of the Granite Harbour Intrusive Complex [*Gunn and Warren*, 1962; *Allibone et al.*, 1993]. Pluton emplacement was followed by uplift and erosion, resulting in the development of the regionally extensive Kukri Peneplain above which deposition of the mainly non-marine Devonian to Triassic Beacon Supergroup took place [*Barrett*, 1991]. During Jurassic, a large magmatic event, both intrusive and effusive, took place along the TAM for more than 3500 km

(Ferrar Large Igneous Province [*Elliot and Fleming*, 2008]).

[7] The southern and eastern sides of the VLB are characterized by the presence of extensive volcanic centers belonging to the Cenozoic (ca. 19 Ma to present) alkaline McMurdo volcanic group. The creation of Ross Island volcanoes resulted in significant modification of the paleogeography of McMurdo Sound and caused an increase of basin subsidence due to flexural loading [*Kyle*, 1981, 1990]. Evidence of older volcanism, possibly dating back to the late Oligocene, has been found within sediments recovered by CIROS-1 and the CRP-2A drill cores [*Smellie*, 2000; *Talarico et al.*, 2000; *Sandroni and Talarico*, 2004] and it was described for West Antarctica Rift System in the Northern Victoria Land region [*Rocchi et al.*, 2002].

[8] The distribution of volcanic centers was controlled by NNE and WNW trending lineament sets which developed starting at ca. 55 Ma and lasting until mid-Miocene time [*Wilson*, 1999; *Fitzgerald*, 2002]. The NNE trending structures consist of normal faults associated with rifting and uplift of the TAM which are segmented into different mountain blocks by WNW trending transfer faults [*Wilson*, 1999]. The Blue, Radian and Pyramid Lineaments, forming the so-called Discovery accommodation zone [*Wilson*, 1999], separate the Royal Society and Skelton blocks and divide the volcanic Mount-Morning-Minna Bluff area from the crystalline basement exposure of the TAM. These tectonic lineaments partly coincide with E–W seafloor spreading in the Adare Trough, northwest of the Ross Sea, which occurred from 46 to 26 Ma [*Cande et al.*, 2000] and are responsible for normal faulting and related tectonic exhumation of the TAM [*Hamilton et al.*, 2001]. The onset of exhumation of the TAM is older, as testified by thermochronology data. In fact, as suggested by *Fitzgerald* [2002], three main periods of post-Jurassic exhumation are recognized: Early Cretaceous (125–110 Ma), Late Cretaceous (100–80 Ma) and early Cenozoic. The onset of the Cenozoic exhumation pulse is placed at c. 55 Ma, but it generally gets younger to the south along the TAM. Recent data obtained by (U-Th)/He dating on either side of the Ferrar Glacier confirmed that the main denudational episode began in the early to mid Eocene [*Fitzgerald et al.*, 2006]. However, no bedrock thermochronological ages are known south of the Blue Lineament up to the central TAM in the region of the Nimrod Glacier, about 500 km southward of the Ross Bay. Here, the last exhumation phase generally began at about 50 Ma, but AFT ages as young as 24 Ma have been detected locally [*Fitzgerald*, 1994; *Fitzgerald and Stump*, 1997; *Miller et al.*, 2010].

3. The AND-2A Drilled Succession

[9] The custom-built drilling system permitted the recovery of a sediment and rock core to 1138.54 m below seafloor (mbsf) with 98% recovery [*Harwood et al.*, 2009]. The ANDRILL sedimentology/stratigraphy team subdivided the core into 14 lithostratigraphic units (LSUs) on the basis of significant lithological changes observed downcore [*Fielding et al.*, 2009]. *Fielding et al.* [2011] and *Passchier et al.* [2011] interpreted the LSUs as due to periodic transitions from subpolar glacial regime to high-latitude temperate wet-based glaciers. In particular, diamictite-dominated facies association at 1138–1040 mbsf (20.2–20.1 Ma), 937–905 mbsf (19.6–19.3 Ma), 786–648 mbsf (18.7–17.6 Ma) and in the upper 259 m (younger than 15.4 Ma) are interpreted as deposited in a cold glacial regime, with larger than modern ice volumes [*Passchier et al.*, 2011]. At 1040–937 mbsf (20.1–19.6 Ma), 905–786 (19.3–18.7 Ma) and 648–259 mbsf (17.6–15.4 Ma), generally mudstone-dominated facies indicate a temperate glacial regime [*Passchier et al.*, 2011]. According to *Fielding et al.* [2011], the interval at 638–607 mbsf (17.35–17.3 Ma) records a further period of ice retreat, which may be associated with the onset of the Mid-Miocene Climatic Optimum (MMCO). The following interval (607–471 mbsf; 17.3–16,7 Ma) records a return to glacially proximal conditions whereas ice-distal conditions, probably related with one of the warm period of the MMCO, are recorded between 471 and 436 mbsf (16.7–16.5 Ma) [*Fielding et al.*, 2011].

4. Material and Methods

[10] This work integrates the data set of *Zattin et al.* [2010] with new AFT analyses on samples from the uppermost 285 m and from bottom of the well and provides new U-Pb and AHe data from selected single apatite grains already dated with AFT analysis (Figure 1). All the new samples belong to coarse-grained sandstones, whereas some of the data presented by *Zattin et al.* [2010] are from sandy conglomerates. After AFT analysis, selected samples were run through U-Pb analysis and, finally, some crystals were extracted from the grain mount and then analyzed by AHe thermochronology.

4.1. U-Pb Analysis

[11] Apatite U-Pb dating was performed by laser ablation multicollector inductively coupled plasma mass spectrometry (LA-MC-ICPMS) at the Arizona LaserChron Center (University of Arizona, Tucson); mass spectrometer, laser set-up, and data reduction are the same as those outlined in *Thomson et al.* [2012] with the addition of NIST SRM 614 glass in the standard mount to correct for ^{204}Pb ion counter gain using a ^{206}Pb/^{204}Pb ratio of 17.842 [*Baker et al.*, 2004].

[12] Fission track mounts were prepared for U-Pb analysis by mounting a neighboring polished epoxy standard mount of similar thickness to the fission track mount. The standard mount contained reference apatite for elemental mass fractionation correction (fragments of gem rough Madagascan apatite), a secondary apatite reference material (apatite from the McClure Mountain syenite), NIST SRM 614 glass used to correct for ion counter gain, and Sri Lanka reference zircon, used to check machine performance.

[13] In this work, for samples 55, 245, ANT 168 and ANT 262, ablation was performed using a 35 μm spot diameter and repeating two or three measurements per crystal with a New Wave UP193HE platform with a New WaveSuperCell and a retrofitted ATL-Lasertechnik 4 ns short pulse 193 nm excimer laser source. For all other samples one ablation per crystal was done using the biggest spot diameter (up to 65 μm) allowed by the size of apatites in each sample, using a Photon Machines Analyte G2 laser ablation platform equipped with HelEx ablation chamber, based on the same ATL-lasertechnik laser source.

[14] Uncertainties are accounted for and propagated separately. Final data reduction and calculation of concordia ages, isochron ages, weighted mean ages (Table 1), and age probability density plots was done using Isoplot [*Ludwig*, 2003].

[15] In this paper, ^{206}Pb/^{238}U age is most appropriate, as it has the lower uncertainty when dealing with ages < ca. 1 Ga (min = 0.01; q1 = 0.02; q2 = 0.04; q3 = 0.13; max = 0.64).

4.2. Fission Track Analysis

[16] Apatite grains were separated from 100 cc bulk samples after careful crushing using heavy liquids and magnetic separation techniques. Mounts of apatites in epoxy were ground and polished to expose planar surfaces within the grains and then etched with 5N HNO_3 at 20°C for 20 s to reveal spontaneous fission tracks. Samples then were irradiated with thermal neutrons in the reactor at the Radiation Center of Oregon State University with a nominal neutron fluence of 9×10^{15} n cm^{-2}. The CN-5 dosimeter was used to measure neutron fluence. After irradiation, induced fission tracks in the low-U muscovite that covered apatite grain mounts and glass dosimeter were revealed by etching in 40% HF at 20°C for 40 min. Apatite FT dates (up to 40 grains per sample) were calculated using the external-detector and the zeta-calibration methods [*Hurford and Green*, 1983] with IUGS age standards (Durango, Fish Canyon and Mount Dromedary apatites [*Hurford*, 1990]) and a value of 0.5 for the $4\pi/2\pi$ geometry correction factor (Table 2). The analyses were subjected to the χ^2 test [*Galbraith*, 1981] to detect whether the data sets contained any extra-Poissonian error. A χ^2 probability of less than 5% denotes a significant spread of single grain dates. The observed grain-age distributions were decomposed into different component populations (or "peak ages") by using the binomial peak-fitting method [*Brandon*, 1996]. This technique is based directly on the bimodal distribution that best represents counting statistics for FT dating. Individual fitted peaks have a mean age and standard error.

4.3. Apatite (U-Th)/He Dating

[17] Apatite (U–Th)/He dating was carried out at the University of Arizona He dating laboratory. After AFT and U-Pb analysis, the apatite grains which satisfy quality requirements (e.g., no inclusions, >75 μm in minimum dimension, etc.) were extracted from the epoxy resin mounts and measured for alpha-ejection correction following methods described in *Reiners et al.* [2007].

[18] Single crystals were loaded into 0.8 mm Nb tubes, and degassed under vacuum by heating with a Nd-YAG laser. The concentration of ^{4}He was determined by ^{3}He isotope dilution and measurement of the ^{4}He/^{3}He ratio through a quadrupole mass spectrometer. U, Th and Sm concentrations were obtained by isotope dilution using an inductively coupled plasma mass spectrometer.

[19] In this data set, application of homogeneous α-ejection correction (HAC) is problematic, not only because grains are polished, but also because some of them are abraded, rounded or partly broken. The HAC applied accounts for grain polishing, as proposed by *Reiners et al.* [2007]. As for grains with

Table 1 (Sample). U-Pb Data [The full Table 1 is available in the HTML version of this article]

Grain	U (ppm)	U/Th	204 (cps)	Pb*/Pbc	%Pbc	$^{206}Pb/^{204}Pb$	$^{207}Pb/^{206}Pb$	±(%)	$^{207}Pb/^{235}U$	±(%)	$^{206}Pb/^{238}U$
Sample 55 (81.89–81.95 mbsl)											
16	17.3	0.6	3435	1.7	37.47	37	0.06065	24.77	0.67308	24.90	0.08048
16_2	25.8	0.4	3556	2.3	30.05	46	0.04917	30.68	0.48149	34.33	0.07103
18_2	30.3	2.5	3635	2.6	27.48	52	0.06636	33.21	0.71798	34.07	0.07847
20_1	13.2	1.2	3118	1.1	47.43	29	0.06191	141.57	0.38285	142.63	0.04485
Sample ANT 168 (168 mbsl)											
1_1	42.1	0.8	2109	4.5	18.25	77	0.05716	11.16	0.46298	12.14	0.05874
1_2	21.1	0.9	2061	3.2	23.60	58	0.05551	12.50	0.59756	13.13	0.07807
2_2	32.4	1.7	1903	4.7	17.40	78	0.05791	18.58	0.60464	18.83	0.07573
2_1	35.3	2.1	1805	5.5	15.48	88	0.05722	18.04	0.59382	18.22	0.07527
3	10.3	4.3	453	7.2	12.21	110	0.03105	61.86	0.35730	63.58	0.08347
5_1	12.1	1.3	2862	1.5	40.63	34	0.13103	39.18	1.66889	39.93	0.09238
5_2	11.8	1.0	2089	1.9	34.17	40	0.10077	24.70	1.23021	25.31	0.08854
10_1	57.7	4.4	1804	8.3	10.71	132	0.05487	16.84	0.56738	17.01	0.07499
10_2	78.3	3.8	1840	11.0	8.35	165	0.05202	4.95	0.53274	5.30	0.07427
24_1	53.8	0.7	1910	4.1	19.42	73	0.05475	17.56	0.29842	18.12	0.03953
24_2	77.9	0.8	1815	5.9	14.50	98	0.04917	13.83	0.24959	14.85	0.03682
27_1	11.5	0.6	1894	2.0	33.68	41	0.11311	16.16	1.26770	18.06	0.08128
27_2	17.9	0.6	2094	2.6	27.89	50	0.07397	30.60	0.79133	32.26	0.07759
34_1	58.7	0.8	1984	4.5	18.07	78	0.05452	11.68	0.31219	11.79	0.04153
34_2	73.5	0.7	2037	5.8	14.68	96	0.04805	10.20	0.29623	10.49	0.04471
38_1	13.5	1.1	732	5.5	15.49	89	0.04701	21.87	0.52349	22.72	0.08076
38_2	28.2	0.8	936	8.7	10.30	134	0.05670	9.87	0.63544	10.30	0.08129
38_3	17.3	1.3	908	5.5	15.28	91	0.07204	28.00	0.84723	28.15	0.08529
39_1	1.9	0.4	2544	0.6	61.69	21	0.18141	69.24	4.04536	70.43	0.16173
39_2	19.5	1.3	1879	3.0	24.81	55	0.08208	50.41	0.75994	50.67	0.06715
40_1	11.8	1.1	1701	1.3	43.38	32	0.14292	27.86	0.80112	29.96	0.04065
40_2	51.7	0.9	1946	2.8	26.26	54	0.06776	12.25	0.26035	14.00	0.02787
Sample ANT262 (262 mbsl)											
1_1	48.6	3.6	3389	4.7	17.65	78	0.05919	11.95	0.64156	12.27	0.07861
1_2	23.7	3.5	3444	2.4	29.74	47	0.06379	23.85	0.68860	24.34	0.07829
4	10.6	0.6	4243	1.1	48.69	28	0.06715	42.81	0.74900	42.91	0.08089
6_1	10.8	1.0	1349	2.6	27.87	50	0.06249	30.31	0.68714	31.21	0.07975
6_2	11.8	1.4	1199	3.0	24.83	56	0.07404	35.24	0.68702	37.40	0.06730
7	36.4	27.9	4279	2.6	27.93	50	0.05999	16.26	0.62071	16.58	0.07504
8_1	15.5	23.4	5812	1.1	47.97	29	0.08721	47.08	1.03314	47.14	0.08592
8_2	27.3	29.4	6022	1.6	37.81	36	0.07566	51.34	0.85875	52.40	0.08232
9_1	29.8	10.7	2391	4.1	19.75	70	0.06675	11.41	0.74880	11.65	0.08136
9_2	33.0	7.4	2313	4.5	18.08	77	0.07504	12.26	0.85423	12.65	0.08256
11_1	5.4	4.9	3147	0.8	54.33	25	0.05273	162.02	0.63226	162.21	0.08696
11_2	2.7	5.5	3258	0.6	64.39	21	0.06210	235.02	0.68142	235.14	0.07958
15_1	9.4	0.6	2490	1.4	41.36	33	0.08345	28.73	0.89671	29.04	0.07794
15_2	40.7	0.7	2062	5.8	14.65	94	0.05534	16.20	0.56066	16.47	0.07348
17_1	45.7	1.4	3645	3.8	20.63	67	0.05881	17.27	0.61013	17.56	0.07524
17_2	53.3	1.5	3338	4.8	17.18	80	0.05675	11.64	0.60695	11.75	0.07757
17_3	67.9	1.2	3632	5.5	15.35	90	0.05941	10.31	0.62950	11.02	0.07684
19_1	82.5	0.6	2566	9.6	9.45	148	0.05652	9.55	0.55766	12.36	0.07155
19_2	32.9	0.6	2509	3.9	20.36	68	0.06625	11.97	0.68256	12.30	0.07472
19_3	67.4	0.6	2709	7.3	12.12	114	0.05380	7.76	0.55356	8.09	0.07463
22_1	55.8	21.0	2803	5.6	15.13	92	0.06152	9.19	0.62900	9.34	0.07415
22_2	50.2	20.2	2934	4.9	17.00	81	0.06166	10.61	0.62756	10.69	0.07381
23_1	43.1	50.7	2803	4.8	17.32	81	0.07552	10.79	0.84585	10.91	0.08123

[a]All uncertainties are reported at the 1-sigma level, and include only measurement errors. U concentration and U/Th are calibrated relative to Madagascar reference apatite and are accurate to ~20%. Common Pb correction is from measured ^{204}Pb with common Pb composition interpreted from *Stacey and Kramers* [1975] and $^{206}Pb/^{238}U$ age through 5 iterative steps. Common Pb composition assigned uncertainties of 1.5 for $^{206}Pb/^{204}Pb$, 0.3 for $^{207}Pb/^{204}Pb$, and 2.0 for $^{208}Pb/^{204}Pb$. Pb*/Pbc = radiogenic Pb/common Pb. Approximate Pb*/Pbc and % Pbc calculated from measured ^{204}Pb, ^{206}Pb and *Stacey and Kramers* [1975] $^{206}Pb/^{204}Pb$ model value at $^{206}Pb/^{238}U$ age. U/Pb and $^{206}Pb/^{207}Pb$ fractionation is calibrated relative to fragments Madagascar reference apatite of 485.0 ± 1.7 Ma (95% conf.). U decay constants and composition as follows: $^{238}U = 9.8485 \times 10^{-10}$, $^{235}U = 1.55125 \times 10^{-10}$, $^{238}U/^{235}U = 137.88$. ^{204}Pb ion counter gain on measured $^{206}Pb/^{204}Pb$ was corrected using NIST614 glass ($^{206}Pb/^{204}Pb$ value of 17.482). bd = below detection (207 signal too low for reliable measurement). cps = counts per second.

10.1029/2012GC004357

Table 2. AFT Data[a]

Sample	Depth (m)	Depositional Age (Ma)	Grains	Spontaneous		Induced		$P(\chi)^2$	Dosimeter		Central Age (Ma) ± 1σ	P1	P2	P3
				ρ_s	N_s	ρ_i	N_i		ρ_d	N_d				
ANT58	58	9.4	16	4.44	428	3.47	3341	0.0	1.24	6481	25.5 ± 2.9	21.9 ± 2.1, 73.7%	37.7 ± 4.2, 26.3%	–
ANT60	60	9.4	13	7.05	658	4.32	4035	0.0	1.33	6942	35.1 ± 3.5	35.1 ± 3.5, 100%	–	–
ANT69	69	9.5	20	4.33	615	2.83	4014	0.0	1.75	7058	33.7 ± 3.5	18.8 ± 3.4, 29.4%	41.3 ± 3.2, 70.6%	–
ANT94	94	10.2	20	3.87	485	2.62	3285	17.0	1.26	6539	31.2 ± 2.7	30.7 ± 2.8, 100%	–	–
ANT118	118	10.8	16	5.62	366	3.74	2439	0.0	1.32	6885	33.6 ± 4.4	21.7 ± 3.2, 53%	47.3 ± 5.1, 47%	–
ANT129	129	11.3	34	4.83	922	3.09	5891	0.0	1.29	6712	37.6 ± 3.9	27.2 ± 2.2, 61%	48.3 ± 6.0, 26.9%	77.0 ± 11.2, 12.1%
ANT138	138	11.7	40	5.10	920	2.86	5157	0.0	1.37	7115	43.3 ± 4.7	28.9 ± 2.5, 60.3%	58.7 ± 5.2, 37.2%	228.6 ± 45.1, 2.5%
ANT168	168	12.5	40	9.75	1458	3.33	5548	0.0	1.30	6769	55.1 ± 4.4	35.9 ± 4.1, 38.6%	67.8 ± 4.6, 61.4%	–
ANT193	193	13.3	20	5.23	388	2.84	2108	0.0	1.22	6366	47.7 ± 12.5	25.6 ± 2.4, 79.9%	191.0 ± 24.6, 20.1%	–
ANT225	225	14.2	38	4.30	597	1.84	2552	0.0	1.28	6654	57.8 ± 9.2	34.6 ± 2.4, 80.6%	226.3 ± 27, 19.4%	–
ANT257	257	15.2	40	3.68	643	1.56	2736	0.0	1.34	7000	58.1 ± 8.5	36.6 ± 3.1, 71.7%	141.1 ± 14.3, 28.3%	–
ANT262	262	15.2	40	7.84	1245	4.53	7198	0.0	1.47	6959	49.5 ± 4.8	26.1 ± 1.7, 39.3%	57.0 ± 2.8, 51.1%	146.5 ± 13.1, 9.6%
ANT284	284	15.3	40	4.37	627	2.30	3293	0.0	1.31	6827	44.8 ± 6.5	18.8 ± 2, 53.5%	64.7 ± 6.9, 37.5%	179.5 ± 27.6, 8.9%
2A-7	1062.5	20.1	25	5.72	338	1.56	919	91.6	1.13	5356	75.7 ± 5.0	75.7 ± 4.9, 100%	–	–

[a]Central ages calculated using dosimeter glass CN5 and ζ-CN5 = 345.54 ± 18.45 (analyst MZ). ρ_s: spontaneous track densities ($\times 10^5$ cm^{-2}) measured in internal mineral surfaces; N_s: total number of spontaneous tracks; ρ_i and ρ_d: induced and dosimeter track densities ($\times 10^6$ cm^{-2}) on external mica detectors (g = 0.5); N_i and N_d: total numbers of tracks; P(χ^2): probability of obtaining χ^2-value for ν degrees of freedom (where ν = number of crystals-1); a probability >5% is indicative of an homogenous population. Samples with a probability <5% have been analyzed with the binomial peak-fitting method.

Table 3. Apatite (U-Th)/He Data

Strat. Age (Ma)	Grain	4He (ncc)	U (ng)	Th (ng)	Th/U (atom.)	Sm (ng)	Raw Age (Ma)	±σ (Ma)	Mass (μg)	mwar[a] (μm)	U (ppm)	Th (ppm)	Sm (ppm)	^{4}He (nmol/g)	eU[b] (ppm)	Grain Shape	HAC[c] Polish. Grain	Lag Time (Raw)	% of HAC Applic.	Fully HAC Corrected Age (Ma)	±σ (Ma)	% HAC Corrected Age (Ma)	±σ (Ma)	Min Age (Ma)	Max Age (Ma)	Plot Age[d] (Ma)	±σ[d] (Ma)
Sample 55																											
9.4	17	0.08	0.02	0.08	5.06	0.36	19.18	0.34	0.99	31.88	15.91	78.41	367.87	3.62	34.33	irr.	0.62	9.78	30	30.98	0.55	22.76	0.41	22.35	31.54	**26.95**	**4.59**
	5	0.22	0.04	0.04	1.19	0.35	39.10	0.83	1.67	33.87	21.54	24.88	212.70	5.85	27.39	irr.	0.68	29.70	16	57.60	1.23	42.12	0.90	41.23	58.82	**50.03**	**9.26**
Sample ANT168																											
12.5	1	0.28	0.04	0.06	1.71	0.25	44.09	0.86	0.72	29.80	51.64	85.93	352.44	17.26	71.84	euhed.	0.59	31.59	100	75.03	1.47	44.09	1.47	73.55	76.50	**75.03**	**1.47**
	19	0.74	0.08	0.08	1.04	0.46	60.84	1.13	1.63	32.56	49.31	49.88	282.49	20.24	61.03	irr.	0.67	48.34	14	91.06	1.70	85.25	1.70	63.71	92.76	**78.23**	**14.52**
	14	0.26	0.04	0.06	1.62	0.20	41.31	0.83	0.62	29.79	60.28	95.36	323.83	18.59	82.69	irr.	0.58	28.81	17	71.73	1.45	63.57	1.45	45.59	73.18	**59.38**	**13.79**
	15	0.65	0.06	0.14	2.50	0.68	60.75	1.06	1.21	34.17	46.13	112.63	564.11	24.16	72.60	irr.	0.66	48.25	14	92.59	1.61	86.47	1.61	63.84	94.20	**79.02**	**15.18**
	20	0.85	0.11	0.17	1.57	0.79	46.82	0.86	1.49	38.55	73.51	112.17	531.79	25.50	99.87	euhed.	0.69	34.32	100	67.40	1.23	46.82	1.23	49.65	68.63	**59.14**	**9.49**
Sample ANT262																											
15.2	25	0.09	0.03	0.09	3.08	0.30	13.33	0.28	1.28	34.28	24.06	72.21	232.86	2.98	41.03	irr.	0.66	−1.87	75	20.24	0.43	14.56	0.43	18.02	20.66	**19.34**	**1.32**
	7	0.06	0.02	0.04	2.17	0.23	18.21	0.39	0.87	27.44	19.87	42.13	267.07	2.96	29.77	euhed.	0.57	3.01	100	32.09	0.68	18.21	0.68	31.41	32.77	**32.09**	**0.68**
	11	0.05	0.02	0.01	0.57	0.06	21.86	0.54	1.32	38.99	13.15	7.26	41.64	1.76	14.85	euhed.	0.69	6.66	100	31.54	0.78	21.86	0.78	30.76	32.32	**31.54**	**0.78**
	15	0.16	0.03	0.07	2.40	0.38	28.61	1.01	0.68	30.46	43.04	100.80	563.22	10.44	66.72	euhed.	0.59	13.41	100	48.91	1.73	28.61	1.73	47.17	50.64	**48.91**	**1.73**
	22	0.29	0.07	0.01	0.12	0.33	34.05	0.98	1.21	35.68	55.69	6.70	270.48	10.60	57.27	irr.	0.68	18.85	30	50.21	1.44	43.90	1.44	37.73	51.65	**44.69**	**6.96**
	28	0.20	0.03	0.06	1.73	0.45	34.44	0.63	0.87	28.97	38.57	64.93	515.88	10.15	53.83	irr.	0.59	19.24	26	58.12	1.07	49.26	1.07	39.77	59.19	**49.48**	**9.71**
	17	1.97	0.21	0.25	1.23	0.70	59.68	1.12	2.60	40.22	81.29	97.43	268.33	33.82	104.19	irr.	0.73	44.48	19	81.26	1.53	76.11	1.53	62.44	82.79	**72.62**	**10.17**
	19	3.31	0.28	0.71	2.57	1.53	60.34	0.98	2.55	46.75	110.74	277.59	600.60	57.88	175.97	irr.	0.75	45.14	19	80.90	1.32	76.03	1.32	63.08	82.21	**72.65**	**9.57**
	6	0.30	0.03	0.03	1.05	0.74	62.35	1.57	1.58	32.09	19.42	19.90	467.35	8.34	24.10	irr.	0.66	47.15	16	94.13	2.36	86.97	2.36	65.69	96.49	**81.09**	**15.40**
	9	0.97	0.11	0.02	0.20	0.43	69.28	1.53	2.04	46.61	53.80	10.74	211.83	21.25	56.33	irr.	0.74	54.08	16	93.49	2.07	88.46	2.07	71.52	95.56	**83.54**	**12.02**
Sample 245																											
18.9	20	0.06	0.02	0.05	2.97	0.50	16.98	2.14	3.24	45.77	5.31	15.36	154.83	0.84	8.92	irr.	0.76	−1.92	84	22.44	2.82	17.65	2.82	18.86	25.26	**22.06**	**3.20**
	2	0.05	0.01	0.05	4.27	0.46	17.48	1.88	5.62	54.69	2.02	8.42	81.65	0.39	4.00	irr.	0.80	−1.42	86	21.96	2.36	17.48	2.36	19.04	24.32	**21.68**	**2.64**
	5	0.50	0.03	0.06	2.39	0.71	100.99	1.71	6.28	54.53	4.13	9.60	112.80	3.58	6.38	euhed.	0.80	82.09	100	125.69	2.13	100.99	2.13	123.56	127.82	**125.69**	**2.13**
	6	0.09	0.03	0.08	3.03	0.68	15.77	0.28	2.05	34.62	13.69	40.39	333.32	2.01	23.18	euhed.	0.69	−3.13	100	22.99	0.41	15.77	0.41	22.58	23.40	**22.99**	**0.41**

[a]Mass-weighted average radius.
[b]Effective U (U + 0.235 Th).
[c]Homogeneous α-ejection correction.
[d]Bold is used for values that have been plotted in Figures 3 and 4.

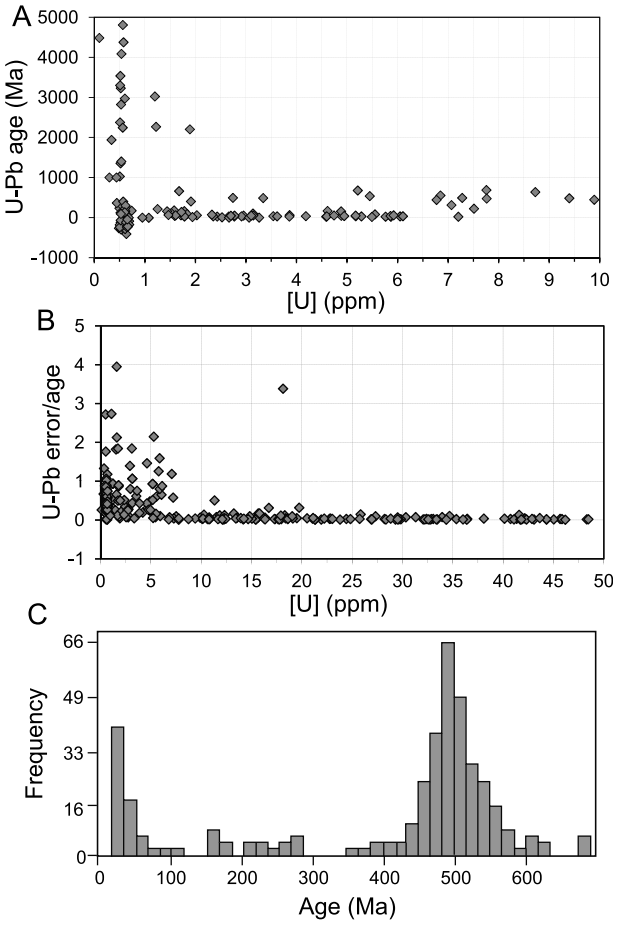

Figure 2. (a) U-Pb age versus U content; anomalously old (≫600 Ma) or young (<0 Ma) ages occur in case of grains with U concentration lower than 0.75 ppm. (b) Relative error versus U content; note the large errors for U concentration lower than 7.5 ppm. *y* axis is adimensional. (c) Histogram representing U-Pb ages considered acceptable.

irregular shape we chose an approach based on *Rahl et al.* [2003]. For such grains we assume that the external rim was lost during transport immediately before deposition, such that the minimum estimate of the period of time during which the analyzed portion of the grain has lost Helium by α-ejection is given by its depositional age (τ_{dep}). Thus the ratio between depositional age and AHe fully corrected age (τ_c) gives an estimate of the minimum period during which He was lost by α-ejection with respect to the period during which He was being produced ($x = \tau_{dep}/\tau_c$). To calculate the minimum age (Table 3) the HAC correction was therefore applied only to the minimum fraction of time during which He loss occurred (i.e., the time since deposition), whereas for the rest of the time no correction was applied.

[20] The minimum age (Min age in Table 3) is therefore calculated as:

$$\tau_{min} = (\tau_r(1-x) + \tau_c x) - (\sigma_r(1-k) + \sigma_c k)$$

where $k = \sigma_{dep}/\sigma_c$.

[21] The upper error bars shown in the plots (Max age in Table 3) are the corrected ages plus their analytical uncertainty, whereas the Plot age is the mean between Min and Max age. For euhedral grains, α-ejection was assumed to have occurred over the whole time the crystal has been accumulating He following cooling through its closure temperature. For these grains a full (100%) HAC is applied.

5. Data

5.1. U-Pb Data

[22] Apatite U-Pb ages are listed in Table 1 and in Figure 2. In this work we present one of the first applications of U-Pb dating on apatites previously dated by fission track analysis, described in *Thomson et al.* [2012]. As expected, the very low U content of many of the analyzed grains strongly affects the analytical precision. Errors higher than 20% occur mainly (except for a few grains) in case of grains with U concentration lower than 7.5 ppm, and anomalously old (≫600 Ma) or young (<0 Ma) ages occur only in case of grains with U concentration lower than 0.75 ppm (Figure 2a). As a consequence only age values referred to grains with U concentration higher than 0.75 ppm are considered acceptable and used for discussion. Moreover, grains with U concentration between 0.75 and 7.5 ppm characterized by extremely high analytical error (age error/age >100%; Figure 2b) were excluded from data discussion. As can be observed in Figure 2c, the resulting data set presents a wide range of age values, spanning from 18 to 690 Ma. Data clearly cluster into two main peaks (Figure 2c). The younger of these yields ages < ca. 45 Ma; the oldest has a larger range but it clusters around 500 Ma. Finally, a few grains yielded U-Pb ages between 200 and 300 Ma, and slightly older than 600 Ma.

5.2. AFT Data

[23] AFT data show multiple peaks in most of the samples. Unfortunately, the small amount of available core material did not allow a large collection of grains. Therefore, counting statistics are often poor

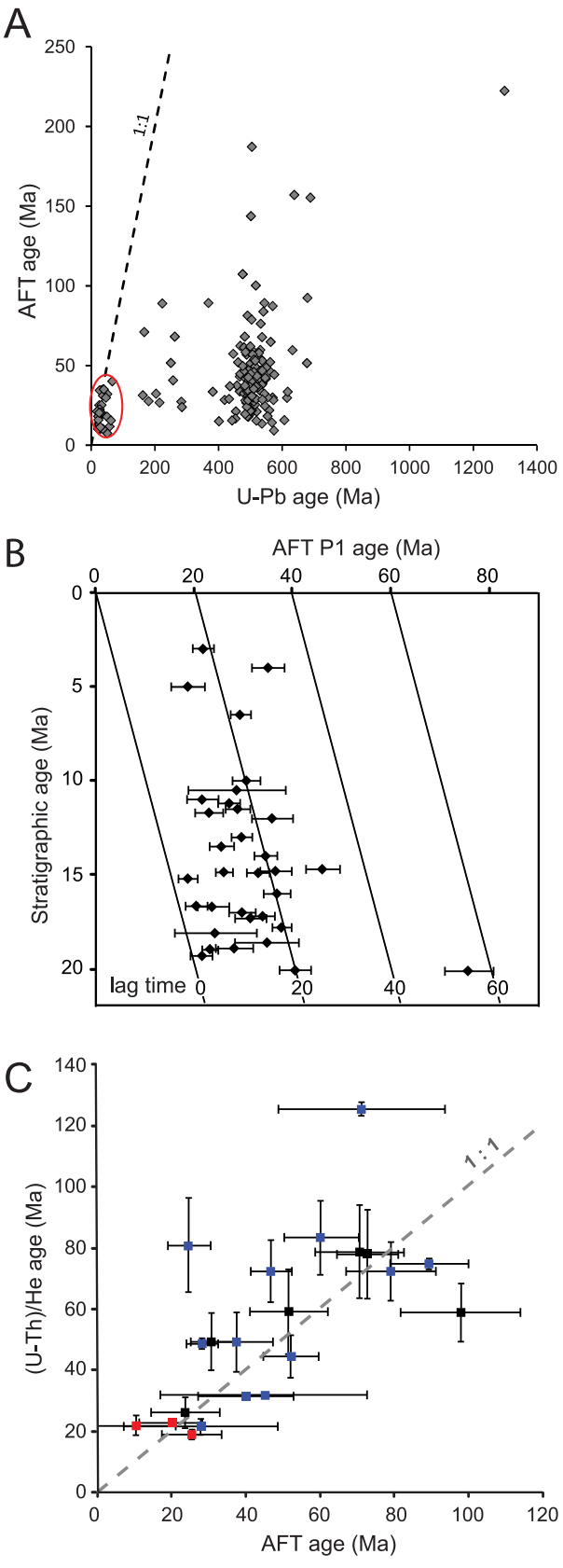

and peak separation is equivocal. Nevertheless, the grain-age distributions are clearly dominated by grains younger than 40 Ma (Table 2 and Figure 3a), confirming the results obtained by *Zattin et al.* [2010]. These grains are grouped in the P1 peak which ranges from 18.8 Ma (sample ANT69) to 36.6 Ma (sample ANT257). In most of the samples the P1 peak contains most if not all of the apatite grains. A noteworthy exception is sample 2A-7, in which a single population with a mean at 75.7 Ma was detected. The overall picture of the AFT ages and more specifically the P1 peak, does not show any particular trend along the sampled succession. Lag time (i.e., the time required for the rock to be exhumed to the surface from the AFT closure temperature of about 100°C, eroded, and then the apatite transported to an adjacent basin assuming that transportation time is geologically instantaneous) for the P1 peak shows quite a wide range of values, up to more than 30 Ma. However, the overall trend shows a decrease of lag time toward the bottom of the sediment core (with exception of the lowermost sample; Figure 3b).

5.3. AHe Data

[24] AHe dating was performed in order to test the efficacy of triple dating and to add constrains on cooling of grains through low temperatures. Only a small percentage of the grains dated by U-Pb and AFT methods were suitable for AHe dating, since they were both polished and laser ablated, thus often being too small or too fragile. Twenty-one apatite grains belonging to four selected samples were dated and the results are presented in Table 3 and Figure 4. Analytical values are generally of good quality, as confirmed by the independence of age and relative error from eU (effective Uranium, quantity typically used to represent the concentration of U and Th; Figure 4). The corrected ages are

Figure 3. (a) Apatite U-Pb versus apatite fission track (AFT) ages for 219 double dated crystals. Red ellipse marks the cluster of grains of possible volcanic origin. (b) Lag-time calculated for youngest AFT peak (P1). Note that value for lowermost sample has been excluded as it is out of scale (ca. 50 m.y.) and that stratigraphic constraints for upper 100 m bsf are very weak. (c) AFT versus apatite (U-Th)/He ages. Red: grains with U-Pb < 40 Ma; blue: grains with U-Pb > 400 Ma; black: grains not dated with U-Pb. AFT data are derived from a combination of the newly presented data and the *Zattin et al.* [2010] data set.

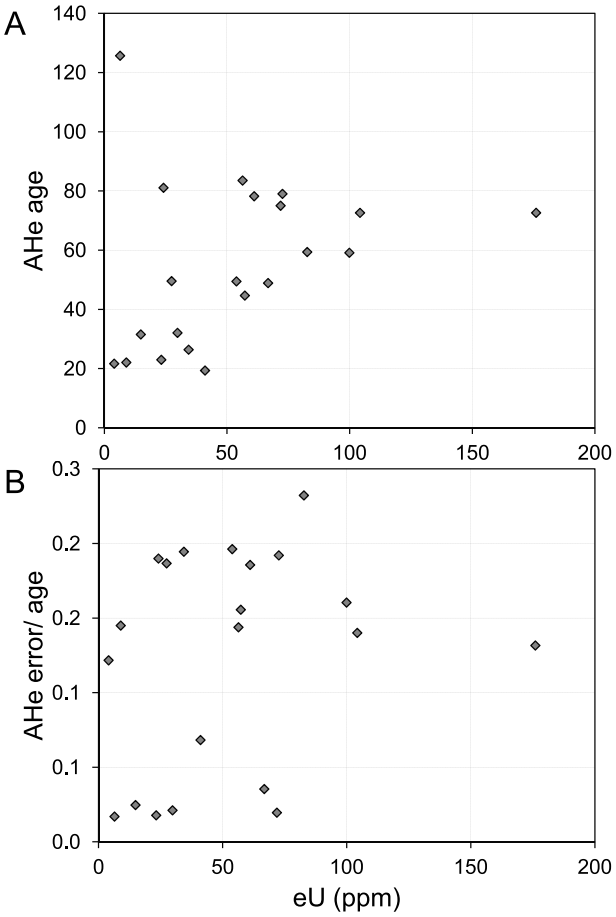

Figure 4. (a) AHe age versus eU (effective uranium concentration, a parameter that weights the decay of the two parents for their alpha productivity, computed as [U] + 0.235[Th]). There is no correlation between these parameters (R^2 = 0.09). (b) Relative error versus eU.

between 19 and 125 Ma, most of them clustering around 40 Ma.

5.4. Integrated Data Set

[25] Figure 3c shows a substantial overlap of AFT and AHe ages, thus suggesting a generally fast cooling through shallow crustal levels. As pointed out earlier, several crystals yield AHe older than AFT age (Data Set S1 in the auxiliary material and Figure 3c), though in most cases the two errors overlap (generally due to high AFT error as a result of the low number of spontaneous tracks).[1] For the cases of a few grains with stronger inversion we suggest that the most likely explanation is that a too-high alpha ejection correction was applied, leading to artificially old AHe ages. Even if crystals showing age inversion could not be used to infer precise thermal histories, they still can be interpreted as overlapping ages, thus pointing to fast cooling through the range 120°–40°C.

[26] Two main age clusters are identified in Figure 3a, the first characterized by U-Pb ages of ca. 500 Ma and AFT ages spanning between ca.120 and 20 Ma, and the second yielding young (average age of 45 Ma) U-Pb ages and AFT ages a few Myr younger.

6. Discussion

6.1. Evidence for a Late Eocene/Early Oligocene Volcanic Event

[27] Our data demonstrate the necessity of using of apatite triple dating to distinguish grains characterized by almost instantaneous (e.g., volcanic) and slow (e.g., due to erosional exhumation) cooling histories. Volcanic apatites are clearly identified by the nearly overlapping crystallization (i.e., U-Pb) and low-temperature thermochronological (i.e., AFT and AHe) ages (Figure 3). At first glance, the discovery of volcanic grains is not surprising given that volcanic rock fragments are very abundant throughout the core [*Panter et al.*, 2008; *Sandroni and Talarico*, 2011; *Talarico and Sandroni*, 2011]. However, before this work, petrological and geochronological data [*Panter et al.*, 2008; *Di Vincenzo et al.*, 2010] indicated that they were mainly sourced from the volcanic centers of the Erebus Volcanic Province, and specifically from the area around present-day Mount Morning, where the oldest known volcanic rocks (ca. 19 Ma) are exposed [*Kelly et al.*, 2008]. However, when looked at in more detail, comparison with available Ar-Ar ages from volcanic deposits on land, suggests that volcanic rocks within the AND-2A core were supplied from the south, possibly with source areas closer to the drill site for the upper core levels, and from 358 m below seafloor downhole, with a "proto-Mount Morning" as the main source [*Di Vincenzo et al.*, 2010]. Actually, dating of tephra layers in previous drill cores in the Cape Roberts area (CRP-1 and CRP-2A) extends the volcanic activity in the area back to the Late Oligocene [*McIntosh*, 1998, 2000]. Our data push further back the time of first appearance of magmatic sources in the area south of the Erebus Volcanic Province as they provide strong evidence for the existence of volcanoes in the late Eocene/early Oligocene. The location of volcanic

[1]Auxiliary materials are available at ftp://ftp.agu.org/apend/gc/2012gc004357.

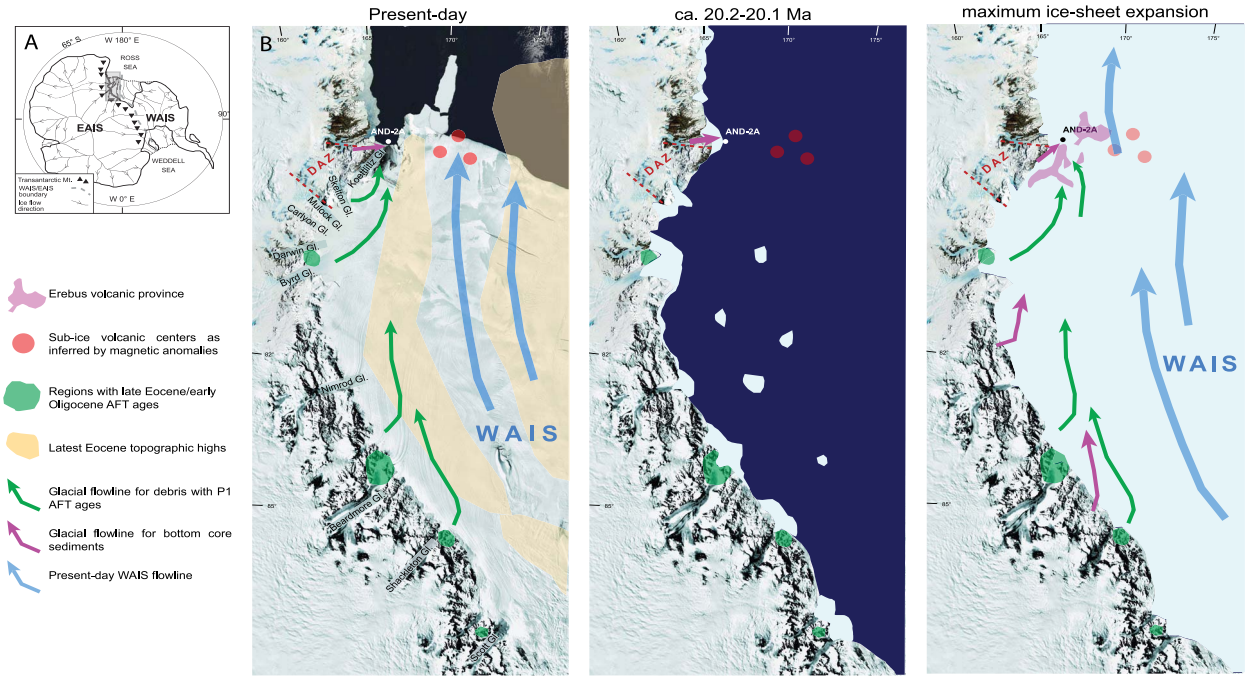

Figure 5. (a) The Antarctic continent with present-day glacial flow lines [after *Drewry*, 1983] and location of Figure 3b (gray box). (b) Schematic representation of sediment dispersal patterns and source areas. Sub-ice volcanic centers as inferred by magnetic anomalies by *Behrendt et al.* [1995, 2004] and *Chiappini et al.* [2002]. There are no detailed data to identify the presence of more volcanic edifices more to the south. The "Latest Eocene topographic high" has been suggested by modeling of *Wilson et al.* [2012] and could represent possible source of apatites deposited at AND-2A site. Regions exhumed in the late Eocene/early Oligocene are constrained by data from *Fitzgerald* [1994], *Miller et al.* [2010], and *Blythe et al.* [2011]. Note that these regions could be slightly larger and no data exist between Koettlitz and Skelton glaciers. DAZ: Discovery Accommodation Zone as defined by *Wilson* [1999].

centers of such age is unknown, but aeromagnetic anomalies suggest the presence of subglacial volcanic centers beneath the Ross Ice Shelf and the WAIS (Figure 5) [*Behrendt et al.*, 1995, 2004; *Chiappini et al.*, 2002]. A submarine-subglacial magnetic anomaly of about the same area as Mount Erebus is located about 100 km offshore of Ross Island and, because of its form, it has been interpreted as a subaerially erupting volcano [*Behrendt et al.*, 1995]. Many other similar anomalies are present below the WAIS more to the south [*Behrendt et al.*, 2004]. Furthermore, the presence of late Eocene-Oligocene magmatism would be consistent with the geodynamic evolution of this part of Antarctica, as it is coeval with the main rift phase. In fact, pluton and dykes ranging from 48 to 23 Ma are widespread in North Victoria Land [*Tonarini et al.*, 1997; *Rocchi et al.*, 2002]. However, it is generally accepted that sediments deposited in the southern VLB follow the ice sheet dynamics and therefore their flow is from south to north [e.g., *Hauptvogel and Passchier*, 2012; *Talarico et al.*, 2011]. Of consequence, a provenance of the volcanic grains from Northern Victoria Land can be excluded.

[28] The near absence of U-Pb ages as well as AFT ages related to the Miocene syndepositional volcanism is noteworthy. A possible explanation is that the composition of magma and the very fine grained volcanic clasts [*Panter et al.*, 2008] prevent the presence of apatite crystals with a significant content of uranium and size large enough to be dated.

6.2. Exhumation and Erosion of the TAM

[29] Most of the U-Pb data show Cambrian-Ordovician ages, obtained from apatites with both P1 and older AFT ages. These data clearly document that most of the dated grains are derived from erosion of late Proterozoic-Cambrian rocks of the TAM. In fact, the main emplacement phase of igneous rocks related to the Ross Orogeny (known as "Granite Harbour Intrusives" [*Borg et al.*, 1987]) is constrained between about 510 and 480 Ma [*Allibone and Wysoczanski*, 2002; *Stump*, 1995;

Bomparola et al., 2007, and references therein]. In the Central Transantarctic Mountains and in Southern Victoria Land, granitic to tonalitic rocks, locally with gneissic texture, yield ages as old as ca. 550 Ma [*Goodge et al.*, 1993; *Cottle and Cooper*, 2006; *Stump et al.*, 2006, and references therein]. However, as there is not a clear trend of crystallization ages along this sector of the TAM and the analytical error on our single grain ages is quite large, the detrital apatite U-Pb data alone do not allow a precise location of the sediment source. A much better fingerprint of potential provenance is provided by our combination of such dates with low-temperature ages from the same grain. Figure 3 shows that most of the grains are derived from bedrock crystallized or metamorphosed during Cambrian-Ordovician times but exhumed only in the Oligocene-Early Miocene. These data contrast with what is known so far from bedrock data from the adjacent TAM as most samples collected in Southern Victoria Land yield much older AFT ages, with only a few samples dated as Late Eocene [*Fitzgerald*, 2002]. However, it is important to note that very few bedrock low-temperature data are known south of the Blue Lineament (preliminary low-T data with ages as young as 31 Ma have been obtained from the Byrd glacier area [*Blythe et al.*, 2011]) up to the central TAM in the region of the Nimrod Glacier (about 500 km away), where AFT ages consistent with our P1 peak have been published [*Fitzgerald*, 1994]. According to *Miller et al.* [2010], more to the south (Shackleton Glacier region) rapid Cenozoic denudation began at about 40 Ma and persisted until ca. 26 Ma.

[30] Our detrital age data can be further discussed in the light of published provenance information obtained from sandstone and gravel clast petrography. Comparison of data from these different methodologies is not univocal as gravel clast abundances may not be representative of the sand fraction because of preferential disaggregation of soft lithologies. Moreover, discussion about relative proportion of age populations in the detrital data set may be strongly biased by different abundance of apatite crystals in the different source rock lithologies [*Moecher and Samson*, 2006]. Therefore, the main implication of our work is the identification of possible source region, as any quantification of relative importance of different source lithologies is not possible.

[31] Apart from volcanic rocks, all the previous papers based on detrital petrographic data point to a general south-to-north flow of sediments. The source is presumed to be outcrops of the TAM exposed along the southern Victoria Land coast. Our data fully support this idea as AFT P1 population suggests a provenance from rocks south of the drilling site. However, localization of source areas is equivocal as different petrographic indicators point to different sources. *Sandroni and Talarico* [2011] were able to distinguish three different basement clast assemblages in the early late Miocene section (778.34–122.86 mbsf): Skelton-derived, Koettlitz-derived and "mixed." The lower part of the core section has also been explored by *Talarico and Sandroni* [2011] who identified again three distinct provenance regions: Koettliz and Blue glaciers, Skelton and Mulock glaciers and the area between the Carlyon and Darwin-Byrd glaciers. A similar distinction was made by *Talarico et al.* [2011] on the basis of petrological investigations on Ca-amphibole-bearing metamorphic clasts. A recent paper by *Hauptvogel and Passchier* [2012], based on characterization of heavy mineral fraction of diamictites and sandstones of the upper 650 m of the AND-2A core, indicated extension of the southern sources to the Queen Maud region. Our data show neither a systematic variation of AFT peaks and U-Pb data through the sedimentary succession nor clear correlation with provenance data inferred by petrography. In other words, the P1 AFT peak is dominant despite major changes in petrological provenance. The overall presence of AFT younger than 40 Ma suggests that a large sector of the TAM was eroded in the late Eocene/early Oligocene (Figure 5). Furthermore, although the large analytical errors prevent a precise estimate of the cooling rates, the overall overlap of AFT and AHe ages point to a rapid exhumation event in this period, thus confirming the data of *Miller et al.* [2010]. This result is also supported by the down-core decrease in lag time for the AFT P1 peak which testifies that the TAM have been in a phase of post-orogenic decay for more than 30 m.y. From the lag-time of the order of 13 m.y. in the uppermost samples, we can estimate a cooling rate in the last 5 m.y. of about 8°C/m.y. (considering a closure temperature of the AFT system at 100°C and a surface temperature of 0°C) which corresponds to exhumation rates of less than 0.3 km/m.y. assuming a geothermal gradient ranging from 25°C/km [e.g., *Gleadow and Fitzgerald*, 1987] to 40°C/km [*White*, 1989]. These rates are comparable to estimates based on bedrock AHe data made by *Miller et al.* [2010] for the Shackleton Glacier area and by *Fitzgerald et al.* [2006] for the Ferrar Glacier area. Further evidence for low exhumation rates comes from the work of *Sugden et al.* [1999], who documented a minimal uplift (67 m) of the Royal

Society Range in the last 8 m.y. (although uplift and exhumation are not necessarily related).

[32] As a whole, these different data sets suggest that a very long sector of the TAM (at least part of the Northern TAM and the Central TAM) was affected by a last exhumation event in the Oligocene, but the related vertical displacements were not uniform along the mountain belt. A major role was played by transverse tectonic lineaments and, between them, the faults related to the Discovery Accommodation Zone [*Wilson*, 1999] which probably divided blocks with different vertical displacements (higher to the south; Figure 5). The Discovery Accommodation Zone is formed by the Royal Society block and the contiguous Skelton block and is interpreted as a structural corridor where the northeast structures are the principal longitudinal normal faults associated with rifting and uplift and the west–northwest structures mark transfer faults that accommodate the structural 'step' in the rift flank [*Wilson*, 1999].

[33] An alternative explanation for the ubiquitous presence of the AFT P1 peak requires the existence of important reworking processes. During major glacial periods, the ice-covered inner continental shelf becomes a zone of net erosion as sediments are transported via subglacial debris zones to the outer-continental shelf [*Bart*, 2003]. Actually, the presence of reworked debris is testified by intraclasts that commonly include clasts of diamictites [*Panter et al.*, 2008; *Talarico et al.*, 2011]. However, the amount of intraformational clasts is not enough to justify the large presence of <40 Ma ages.

[34] A remarkable absence of grains with AFT P1 ages is seen in the lowermost sample, collected at 1062.5 mbsf. Gravel petrography data suggest that source of sediments below 1040.28 mbsf is the region around the Koettlitz and Blue glaciers [*Talarico and Sandroni*, 2011]. This area is considered the northern margin of the Discovery Accommodation Zone and, although no bedrock AFT data exist so far, we can envisage that it marks the transition between blocks with different vertical displacements during the last 30–40 m.y. The AFT ages of about 70 Ma are thus apparently a signature for provenance from the Koettlitz/Blue glacier areas, although a source located more to the south cannot be excluded, as *Miller et al.* [2010] detected similar ages in Shackleton glacier area (Figure 5). The work of *Miller et al.* [2010] also shows a general age-elevation correlation (with younger ages at the bottom of the vertical profile as it is expected from the exhumation of a AFT partial annealing zone) so AFT P1 ages could possibly derive from low elevations areas inside Koettlitz/Blue glacier block.

[35] Finally, we point to the possible existence of an emerged ridge in the Ross Ice Shelf adjacent to the TAM in the Oligocene now seen as the buried Coulman high and Central high (Figure 5b) [*De Santis et al.*, 1995; *Wilson and Luyendyk*, 2009; *Wilson et al.*, 2012]. *Brancolini et al.* [1995] and *De Santis et al.* [1995], utilize regional stratigraphic maps and seismic facies analyses to postulate that during the late Oligocene/early Miocene the Central high was partly exposed and partly covered by small subpolar ice caps. At time of deposition of the oldest sediments drilled in the AND-2A core, these topographic highs were probably already eroded but we cannot rule out the possibility that the derived detritus (with Oligocene or older inferred AFT ages) could have fed the investigated basin sequence.

6.3. Implications for Ice-Flow Dynamics

[36] Facies association testifies to the existence of two distinct glacial scenarios: the presence of massive diamictite indicates proximity of the grounding line during glacial maxima, whereas stratified diamictites and biosiliceous facies indicate generally open marine conditions [*Passchier et al.*, 2011]. Glacially dominated conditions with only brief periods of ice retreat occurred at 20.2–20.1 Ma, 19.6–19.3 Ma, 18.7–17.6 Ma and later than 15.4 Ma, with the ice sheet grounded on the shelf near the drill site at ca. 19.4 Ma, 18.6 Ma and 17.6 Ma [*Passchier et al.*, 2011]. During periods of maximum ice sheet expansion, a large part of the McMurdo Sound region was invaded by the WAIS. The EAIS was not large enough to overtop the TAM [*Bart*, 2003], although outlet glaciers along TAM provided some ice volume to the main south-to-north flow which, forced to run close to the southern Victoria Land coastline, would have exerted a dam effect on the lateral inputs (Figure 5). As discussed in the previous section, detrital ages and petrographic data agree with the idea of an ice pattern dominated by south to north trending flow lines parallel to the TAM front.

[37] Koettlitz-Blue glacier provenance in the lowermost section (1138-5-1040.28 mbsf, mostly represented by thick diamictite strata), suggested by *Talarico and Sandroni* [2011] and here confirmed

by AFT data, is therefore partly in conflict with this view as it implies sediment supply from local lobes flowing from W to E. The same conclusion was drawn by *Florindo et al.* [2005] for correlative strata in the CRP-1 well more to the north. This apparent contradiction can be best explained by the presence of outlet glaciers with dominantly W-E flow in a Ross Embayment mostly free of ice [*Dunbar et al.*, 2008; *Talarico and Sandroni*, 2011]. However, in such conditions, one should also expect the presence of ice-rafted debris, with clasts and pebbles derived from alpine glacial systems well south of the drilling site. According to *Hauptvogel and Passchier* [2012], ice-rafted debris could have had its source in the southern TAM during periods of advance of grounding line of EAIS outlet glaciers to the coast.

7. Conclusions

[38] Single grain triple dating of detrital apatites from the AND-2A drill core provides critical new information on the thermal history of source rocks and hence on provenance and dispersal patterns across the Ross Sea during the last 20 m.y. As a whole, these data allow us to identify both erosional and magmatic events active in the source regions. In particular, the discovery of volcanic apatites with a late Eocene/Oligocene age documents the existence of a so far undetected volcanic source well before the Mount Morning magmatic province. The location of the volcanic center is unknown, but aeromagnetic anomalies suggest the presence of subglacial volcanic centers beneath the Ross Ice Shelf and the WAIS.

[39] The overall presence of apatites with AFT ages younger than bedrock ages detected on the adjacent Transantarctic Mountains suggests that most of the apatite-bearing sediments are derived from the region south of the Discovery Accommodation Zone with only a minor contribution from the much closer glaciers of the Royal Society Range. The small gap between AFT and AHe ages indicates that a moderate-to-fast cooling event occurred along this region of the TAM during the Oligocene, after which the chain has been in a post-orogenic decay, with cooling rates of the order of 0.1 km/Ma.

[40] The prevalence of S to N flow implies a major role of the WAIS with large volume of ice grounded at the regional scale in the Ross Embayment. Advance of EAIS-related outlet paleoglaciers into the Ross Sea was dammed by main S to N flow for most of the time. Transport of sediments to the drilling site from Royal Society Range was therefore inhibited and possible only when the Ross Sea was free of ice.

Acknowledgments

[41] Yvonne Cook is thanked for providing apatite separates. Mark Pecha and Nicky Geisler are thanked for supervision during U-Pb analysis at the Arizona LaserChron Center. The article greatly benefited from thorough and constructive reviews by Cornelia Spiegel and Maria Laura Balestrieri. This work has been supported by "Fondazione Cassa di Risparmio di Padova e Rovigo" (Bando Progetti di Eccellenza 2009/2010; Zattin) and PRIN 2008 (Talarico). The ANDRILL (Antarctic geologic drilling) Program is a multinational collaboration between the Antarctic programs of Germany, Italy, New Zealand, and the United States.

References

Acton, G., et al. (2008), Preliminary integrated chronostratigraphy of the AND-2A Core, ANDRILL Southern McMurdo Sound Project, Antarctica, *Terra Antart.*, *15*, 211–220.

Allibone, A., and R. Wysoczanski (2002), Initiation of magmatism during the Cambrian–Ordovician Ross orogeny in southern Victoria Land, Antarctica, *Geol. Soc. Am. Bull.*, *114*, 1007–1018, doi:10.1130/0016-7606(2002)114<1007:IOMDTC>2.0.CO;2.

Allibone, A. H., S. C. Cox, I. J. Graham, R. W. Smillie, R. D. Johnstone, S. G. Ellery, and K. Palmer (1993), Granitoids of the Dry Valleys area, southern Victoria Land, Antarctica: Plutons, field relationships, and isotopic dating, *N. Z. J. Geol. Geophys.*, *36*, 281–297, doi:10.1080/00288306.1993.9514576.

Baker, J., D. Peate, T. Waight, and C. Meyzen (2004), Pb isotopic analysis of standards and samples using a Pb-207-Pb-204 double spike and thallium to correct for mass bias with a double-focusing MC-ICP-MS, *Chem. Geol.*, *211*, 275–303, doi:10.1016/j.chemgeo.2004.06.030.

Barrett, B. E., K. W. Nicholls, T. Murray, A. M. Smith, and D. G. Vaughan (2009), Rapid recent warming on Rutford Ice Stream, West Antarctica, from borehole thermometry, *Geophys. Res. Lett.*, *36*, L02708, doi:10.1029/2008GL036369.

Barrett, P. J. (1991), The Devonian to Triassic Beacon Supergroup of the Transantarctic Mountains and correlatives in other parts of America, in *The Geology of Antarctica*, *Monogr. on Geol. and Geophys.*, vol. 17, edited by R. J. Tingey, pp. 120–152, Oxford Univ. Press, Oxford, U. K.

Bart, P. J. (2003), Were West Antarctic Ice Sheet grounding events in the Ross Sea a consequence of East Antarctic Ice Sheet expansion during the middle Miocene?, *Earth Planet. Sci. Lett.*, *216*, 93–107, doi:10.1016/S0012-821X(03)00509-0.

Behrendt, J. C., D. D. Blankenship, D. Damaske, and A. K. Cooper (1995), Glacial removal of late Cenozoic subglacially emplaced volcanic edifices by the West Antarctic Ice Sheet, *Geology*, *23*, 1111–1114, doi:10.1130/0091-7613(1995)023<1111:GROLCS>2.3.CO;2.

Behrendt, J. C., D. D. Blakenship, D. L. Morse, and R. E. Bell (2004), Shallow-source aeromagnetic anomalies observed over the West Antarctic Ice Sheet compared with coincident bed topography from radar ice sounding—New evidence for glacial "removal" of subglacially erupted late Cenozoic

rift-related volcanic edifices, *Global Planet. Change*, *42*, 177–193, doi:10.1016/j.gloplacha.2003.10.006.

Blythe, A. E., A. D. Huerta, and E. Utevsky (2011), Evaluating the Mesozoic West Antarctic Plateau collapse hypothesis: Results from apatite fission-track and (U-Th)/He analyses from Byrd Glacier Outlet, Abstract T23H-08 presented at 2011 Fall Meeting, AGU, San Francisco, Calif., 5–9 Dec.

Bomparola, R. M., C. Ghezzo, E. Belousova, W. L. Griffin, and S. Y. O'Reilly (2007), Resetting of the U-Pb zircon system in Cambro-Ordovician intrusives of the Deep Freeze Range, northern Victoria Land, Antarctica, *J. Petrol.*, *48*, 327–364, doi:10.1093/petrology/egl064.

Borg, S. G., D. J. DePaolo, E. D. Wendlandt, and T. G. Drake (1987), Studies of granites and metamorphic rocks, Byrd Glacier area, *Antarct. J. U. S.*, *24*, 19–21.

Brancolini, G., A. K. Cooper, and F. Coren (1995), Seismic facies and glacial history in the western Ross Sea (Antarctica), in *Geology and Seismic Stratigraphy of the Antarctic Margin*, *Antarct. Res. Ser.*, vol. 68, edited by A. K. Cooper, P. F. Barker, and G. Brancolini, pp. 209–233, AGU, Washington, D. C.

Brandon, M. T. (1996), Probability density plot for fission-track grain-age samples, *Radiat. Meas.*, *26*, 663–676, doi:10.1016/S1350-4487(97)82880-6.

Cande, S. C., J. M. Stock, D. Müller, and T. Ishihara (2000), Cenozoic motion between East and West Antarctica, *Nature*, *404*, 145–150, doi:10.1038/35004501.

Chiappini, M., F. Ferraccioli, E. Bozzo, and D. Damaske (2002), Regional compilation and analysis of aeromagnetic anomalies for the Transantarctic Mountains–Ross Sea sector of the Antarctic, *Tectonophysics*, *347*, 121–137, doi:10.1016/S0040-1951(01)00241-4.

Cook, Y. A., and D. Craw (2002), Neoproterozoic structural slices in the Ross Orogen, Skelton Glacier area, South Victoria Land, Antarctica, *N. Z. J. Geol. Geophys.*, *45*, 133–143, doi:10.1080/00288306.2002.9514965.

Cooper, A. K., and F. J. Davey (1985), Episodic rifting of the Phanerozoic rocks of the Victoria Land basin, western Ross Sea, *Antarct. Sci.*, *229*, 1085–1087.

Cottle, J. M., and A. F. Cooper (2006), Geology, geochemistry, and geochronology of an A-type granite in the Mulock Glacier area, southern Victoria Land, Antarctica, *N. Z. J. Geol. Geophys.*, *49*, 191–202, doi:10.1080/00288306.2006.9515159.

De Santis, L., J. B. Anderson, G. Brancolini, and I. Zayatz (1995), Seismic record of Late Oligocene through Miocene glaciation on the central and eastern continental shelf of the Ross Sea, in *Geology and Seismic Stratigraphy of the Antarctic Margin*, *Antarct. Res. Ser.*, vol. 68, edited by A. K. Cooper, P. F. Barker, and G. Brancolini, pp. 235–260, AGU, Washington, D. C.

Di Vincenzo, G., L. Bracciali, P. Del Carlo, K. Panter, and S. Rocchi (2010), ^{40}Ar–^{39}Ar dating of volcanogenic products from the AND-2A core (ANDRILL Southern McMurdo Sound Project, Antarctica): Correlations with the Erebus Volcanic Province and implications for the age model of the core, *Bull. Volcanol.*, *72*, 487–505, doi:10.1007/s00445-009-0337-z.

Drewry, D. J. (1983), *Antarctica: Glaciological and Geophysical Folio*, Scott Polar Res. Inst., Univ. of Cambridge, Cambridge, U. K.

Dunbar, G. B., T. R. Naish, P. J. Barrett, C. R. Fielding, and R. D. Powell (2008), Constraining the amplitude of late Oligocene bathymetric changes in Western Ross Sea during orbitally induced oscillations in the East Antarctic Ice Sheet: (1) Implications for glacimarine sequence stratigraphic models, *Paleogeogr. Palaeoclimatol. Palaeoecol.*, *260*, 50–65, doi:10.1016/j.palaeo.2007.08.018.

Elliot, D. H., and T. H. Fleming (2008), Physical volcanology and geological relationships of the Jurassic Ferrar Large Igneous Province, Antarctica, *J. Volcanol. Geotherm. Res.*, *172*, 20–37, doi:10.1016/j.jvolgeores.2006.02.016.

Fahnestock, M. A., T. A. Scambos, R. A. Bindschadler, and G. Kvaran (2000), A millennium of variable ice flow recorded by the Ross Ice Shelf, Antarctica, *J. Glaciol.*, *46*, 652–664, doi:10.3189/172756500781832693.

Fielding, C. R., S. A. Henrys, and T. J. Wilson (2006), Rift history of thewestern Victoria Land Basin: A new perspective based on integration of cores with seismic reflection data, in *Antarctica: Contributions to Global Earth Sciences*, edited by D. K. Futterer et al., pp. 309–318, Springer, Berlin.

Fielding, C. R., J. Whittaker, S. A. Henrys, T. J. Wilson, and T. R. Naish (2008), Seismic facies and stratigraphy of the Cenozoic succession in McMurdo Sound, Antarctica: Implications for tectonic, climatic and glacial history, *Paleogeogr. Palaeoclimatol. Palaeoecol.*, *260*, 8–29.

Fielding, C. R., et al. (2009), Sedimentology and stratigraphy of the AND-2A core, ANDRILL Southern McMurdo Sound project, Antarctica, *Terra Antart.*, *15*, 77–112.

Fielding, C. R., G. H. Browne, B. Field, F. Florindo, D. M. Harwood, L. A. Krissek, R. H. Levy, K. S. Panter, S. Passchier, and S. F. Pekar (2011), Sequence stratigraphy of the ANDRILL AND-2A drillcore, Antarctica: A long-term, ice-proximal record of Early to Mid-Miocene climate, sea-level and glacial dynamism, *Paleogeogr. Palaeoclimatol. Palaeoecol.*, *305*, 307–351, doi:10.1016/j.palaeo.2011.03.026.

Findlay, R. H., D. N. B. Skinner, and D. Craw (1984), Lithostratigraphy and structure of the Koettlitz Group, McMurdo Sound, Antarctica, *N. Z. J. Geol. Geophys.*, *27*, 513–536, doi:10.1080/00288306.1984.10422270.

Fitzgerald, P. G. (1994), Thermochronologic constraints on post-Paleozoic tectonic evolution of the central Transantarctic Mountains, Antarctica, *Tectonics*, *13*, 818–836, doi:10.1029/94TC00595.

Fitzgerald, P. G. (2002), Tectonics and landscape evolution of the Antarctic plate since the breakup of Gondwana, with an emphasis on the West Antarctic Rift System and the Transantarctic Mountains, *R. Soc. N. Z. Bull.*, *35*, 453–469.

Fitzgerald, P. G., and E. Stump (1997), Cretaceous and Cenozoic episodic denudation of the Transantarctic Mountains, Antarctica: New constraints from apatite fission track thermochronology in the Scott Glacier region, *J. Geophys. Res.*, *102*, 7747–7765, doi:10.1029/96JB03898.

Fitzgerald, P. G., S. L. Baldwin, L. E. Webb, and P. B. O'Sullivan (2006), Interpretation of (U–Th)/He single grain ages from slowly cooled crustal terranes: A case study from the Transantarctic Mountains of southern Victoria Land, *Chem. Geol.*, *225*, 91–120, doi:10.1016/j.chemgeo.2005.09.001.

Florindo, F., G. S. Wilson, A. P. Roberts, L. Sagnotti, and K. L. Verosub (2005), Magnetostratigraphic chronology of a late Eocene to early Miocene glacimarine succession from the Victoria Land Basin, Ross Sea, Antarctica, *Global Planet. Change*, *45*, 207–236, doi:10.1016/j.gloplacha.2004.09.009.

Galbraith, R. F. (1981), On statistical models for fission track counts, *Math. Geol.*, *13*, 471–478, doi:10.1007/BF01034498.

Gleadow, A. J. W., and P. G. Fitzgerald (1987), Uplift history and structure of the Transantarctic Mountains: New evidence from fission track dating of basement apatites in the Dry

Valleys area, southern Victoria Land, *Earth Planet. Sci. Lett.*, *82*, 1–14, doi:10.1016/0012-821X(87)90102-6.

Goodge, J., V. Hansen, S. Peacock, B. Smith, and N. Walker (1993), Kinematic evolution of the Miller Range Shear Zone, Central Transantarctic Mountains, Antarctica, and implications for Neoproterozoic to Early Paleozoic tectonics of the East Antarctic Margin of Gondwana, *Tectonics*, *12*(6), 1460–1478, doi:10.1029/93TC02192.

Gunn, B. M., and G. Warren (1962), Geology of Victoria Land between the Mawson and Mulock Glaciers, Antarctica, *N. Z. J. Geol. Geophys.*, *5*, 407–426, doi:10.1080/00288306.1962.10420097.

Hambrey, M. J., P. J. Barrett, and R. D. Powell (2002), Late Oligocene and early Miocene glacimarine sedimentation in the SW Ross Sea, Antarctica: The record from offshore drilling, in *Glacier-Influenced Sedimentation on High-Latitude Continental Margins*, edited by J. A. Dowdeswell and C. O. Cofaigh, *Geol. Soc. Spec. Publ.*, *203*, 105–128.

Hamilton, R., B. Luyendyk, C. Sorlien, and L. Bartek (2001), Cenozoic tectonics of the Cape Roberts Rift Basin and Transantarctic Mountains Front, Southwestern Ross Sea, Antarctica, *Tectonics*, *20*(3), 325–342, doi:10.1029/2000TC001218.

Harwood, D. M., F. Florindo, F. M. Talarico, and R. H. Levy (2009), *Studies From the ANDRILL Southern McMurdo Sound Project, Antarctica. Initial Science Report on AND-2A*, *Terra Antart.*, *15*, 235 pp.

Hauptvogel, D. W., and S. Passchier (2012), Early Middle Miocene (17–14 Ma) Antarctic ice dynamics reconstructed from the heavy mineral provenance in the AND-2A drill core, Ross Sea, Antarctica, *Global Planet. Change*, *82–83*, 38–50, doi:10.1016/j.gloplacha.2011.11.003.

Haywood, A. M., et al. (2009), Middle Miocene to Pliocene history of Antarctica and the Southern Ocean, in *Antarctic Climate Evolution*, *Dev. Earth Environ. Sci.*, vol. 8, edited by F. Florindo and M. Siegert, pp. 401–463, Elsevier, Amsterdam, doi:10.1016/S1571-9197(08)00010-4.

Henrys, S. A., T. J. Wilson, J. M. Whittaker, C. R. Fielding, J. Hall, and T. R. Naish (2007), Tectonic history of mid-Miocene to present southern Victoria Land Basin, inferred from seismic stratigraphy in McMurdo Sound, Antarctica, *U.S. Geol. Surv. Open File Rep.*, *2007-1047*, 4 pp., doi:10.3133/of2007-1047.srp049.

Hurford, A. J. (1990), International Union of Geological Sciences Subcommission on Geochronology recommendation for the standardization of fission track dating calibration and data reporting, *Nucl. Tracks*, *17*, 233–236, doi:10.1016/1359-0189(90)90040-5.

Hurford, A. J., and P. F. Green (1983), The zeta age calibration of fission track dating, *Isot. Geosci.*, *1*, 285–317.

Kelly, P. J., P. R. Kyle, N. W. Dunbar, and K. W. W. Sims (2008), Geochemistry and mineralogy of the phonolite lava lake, Erebus volcano, Antarctica: 1972–2004 and comparison with older lavas, *J. Volcanol. Geotherm. Res.*, *177*, 589–605, doi:10.1016/j.jvolgeores.2007.11.025.

Kyle, P. R. (1981), Glacial history of the McMurdo Sound area as indicated by the distribution and nature of McMurdo Volcanic Group rocks, in *Dry Valley Drilling Project*, *Antarct. Res. Ser.*, vol. 33, edited by L. D. McGinnis, pp. 403–412, AGU, Washington, D. C., doi:10.1029/AR033p0403.

Kyle, P. R. (1990), McMurdo Volcanic Group, western Ross Embayment, in *Volcanoes of the Antarctic Plate and Southern Oceans*, *Antarct. Res. Ser.*, vol. 48, edited by W. E. Le Masurier and J. W. Thomson, pp. 18–145, AGU, Washington, D. C., doi:10.1029/AR048p0018.

Ludwig, K. R. (2003), User's manual for Isoplot 3.00: A Geochronological Toolkit for Microsoft Excel, Berkeley Geochronol. Cent., Berkeley, Calif.

McIntosh, W. C. (1998), $^{40}Ar/^{39}Ar$ geochronology of volcanic clasts and pumice in CRP-1 core, Cape Roberts, Antarctica, *Terra Antart.*, *5*, 683–690.

McIntosh, W. C. (2000), $^{40}Ar/^{39}Ar$ geochronology of tephra and volcanic clasts in CRP-2A, Victoria Land Basin, Antarctica, *Terra Antart.*, *7*, 621–630.

Miller, S. R., P. G. Fitzgerald, and S. L. Baldwin (2010), Cenozoic range-front faulting and development of the Transantarctic Mountains near Cape Surprise, Antarctica: Thermochronologic and geomorphologic constraints, *Tectonics*, *29*, TC1003, doi:10.1029/2009TC002457.

Moecher, D. P., and S. D. Samson (2006), Differential zircon fertility of source terranes and natural bias in the detrital zircon record: Implications for sedimentary provenance analysis, *Earth Planet. Sci. Lett.*, *247*, 252–266, doi:10.1016/j.epsl.2006.04.035.

Naish, T. R., et al. (2008), Late Neogene climate history of the Ross Embayment from the AND-1B drill core: Culmination of three decades of Antarctic margin drilling, in *Antarctica: A Keystone in a Changing World—Proceedings of the 10th International Symposium on Antarctic Earth Sciences*, edited by A. Cooper et al., pp. 71–82, Natl. Acad. Press, Washington, D. C.

Naish, T., et al. (2009), Obliquity-paced Pliocene West Antarctic ice sheet oscillations, *Nature*, *458*, 322–328, doi:10.1038/nature07867.

Panter, K. S., et al. (2008), Petrologic and geochemical composition of the AND-2A core, ANDRILL Southern McMurdo Sound Project, Antarctica, *Terra Antart.*, *15*, 147–192.

Passchier, S., G. Browne, B. Field, C. R. Fielding, L. A. Krissek, K. Panter, S. F. Pekar, and ANDRILL-SMS Science Team (2011), Early and middle Miocene Antarctic glacial history from the sedimentary facies distribution in the AND-2A drill hole, Ross Sea, Antarctica, *Geol. Soc. Am. Bull.*, *123*, 2352–2365, doi:10.1130/B30334.1.

Pollard, D., and R. M. DeConto (2009), Modelling West Antarctic ice sheet growth and collapse through the past five million years, *Nature*, *458*, 329–332, doi:10.1038/nature07809.

Rahl, J. M., P. W. Reiners, I. H. Campbell, S. Nicolescu, and C. M. Allen (2003), Combined single-grain (U-Th)/He and U/Pb dating of detrital zircons from the Navajo Sandstone, *Utah Geol.*, *31*, 761–764, doi:10.1130/G19653.1.

Reiners, P. W., S. N. Thomson, D. McPhillips, R. A. Donelick, and J. J. Roering (2007), Wildfire thermochronology and the fate and transport of apatite in hillslope and fluvial environments, *J. Geophys. Res.*, *112*, F04001, doi:10.1029/2007JF000759.

Rocchi, S., P. Armienti, M. D'Orazio, S. Tonarini, J. R. Wijbrans, and G. Di Vincenzo (2002), Cenozoic magmatism in the western Ross Embayment: Role of mantle plume versus plate dynamics in the development of the West Antarctic Rift System, *J. Geophys. Res.*, *107*(B9), 2195, doi:10.1029/2001JB000515.

Sandroni, S., and F. M. Talarico (2004), Petrography and provenance of basement clasts in CIROS-1 core, McMurdo Sound, Antarctica, *Terra Antart.*, *11*, 93–114.

Sandroni, S., and F. M. Talarico (2011), The record of Miocene climatic events in AND-2A drill core (Antarctica): Insights from provenance analyses of basement clasts, *Global Planet. Change*, *75*, 31–46, doi:10.1016/j.gloplacha.2010.10.002.

Smellie, J. L. (2000), Erosional history of the Transantarctic Mountains deduced from sand grain detrital modes in CRP-

2/2A, Victoria Land Basin, Antarctica, *Terra Antart.*, *7*, 545–552.

Stacey, J. S., and J. D. Kramers (1975), Approximation of terrestrial lead isotope evolution by a 2-stage model, *Earth Planet. Sci. Lett.*, *26*, 207–221, doi:10.1016/0012-821X(75)90088-6.

Stump, E. (1995), *The Ross Orogen of the Transantarctic Mountains*, 284 pp., Cambridge Univ. Press, Cambridge, U. K.

Stump, E., B. F. Gootee, and F. M. Talarico (2006), Tectonic model for development of the Byrd Glacier discontinuity and surrounding regions of the Transantarctic Mountains during the Neoproterozoic–Early Paleozoic, in *Antarctica: Contributions to Global Earth Sciences*, edited by D. K. Fütterer et al., pp. 181–190, Springer, Berlin, doi:10.1007/3-540-32934-X_22.

Sugden, D., and G. Denton (2004), Cenozoic landscape evolution of the Convoy Range to Mackay Glacier area, Transantarctic Mountains: Onshore to offshore synthesis, *Geol. Soc. Am. Bull.*, *116*, 840–857, doi:10.1130/B25356.1.

Sugden, D. E., D. R. Marchant, and G. H. Denton (1993), The case for a stable East Antarctic Ice Sheet, *Geogr. Ann.*, *75*, 151–154, doi:10.2307/521199.

Sugden, D. E., M. A. Summerfield, G. H. Denton, T. I. Wilch, W. C. McIntosh, D. R. Marchant, and R. H. Rutford (1999), Landscape development in the Royal Society Range, southern Victoria Land, Antarctica: Stability since the mid-Miocene, *Geomorphology*, *28*, 181–200, doi:10.1016/S0169-555X(98)00108-1.

Talarico, F. M., and S. Sandroni (2011), Early Miocene basement clasts in ANDRILL AND-2A core and their implications for paleoenvironmental changes in the McMurdo Sound region (western Ross Sea, Antarctica), *Global Planet. Change*, *78*, 23–35, doi:10.1016/j.gloplacha.2011.05.002.

Talarico, F. M., S. Sandroni, C. R. Fielding, and C. Atkins (2000), Variability, petrography and provenance of basement clasts in core from CRP-2/2A, Victoria Land Basin, Antarctica, *Terra Antart.*, *7*, 529–544.

Talarico, F. M., D. Pace, and S. Sandroni (2011), Amphibole-bearing metamorphic clasts in ANDRILL AND-2A core: A provenance tool to unravel the Miocene glacial history in the Ross Embayment (western Ross Sea, Antarctica), *Geosphere*, *7*, 922–937, doi:10.1130/GES00653.1.

Thomson, S. N., G. E. Gehrels, J. Ruiz, and R. Buchwaldt (2012), Routine low-damage apatite U-Pb dating using laser ablation–multicollector–ICPMS, *Geochem. Geophys. Geosyst.*, *13*, Q0AA21, doi:10.1029/2011GC003928.

Tonarini, S., S. Rocchi, P. Armienti, and F. Innocenti (1997), Constraints on timing of Ross Sea rifting inferred from Cainozoic intrusions from northern Victoria Land, Antarctica, in *The Antarctic Region: Geological Evolution and Processes*, edited by C. A. Ricci, pp. 511–521, Terra Antarct., Siena, Italy.

White, P. (1989), Downhole logging, in *Antarctic Cenozoic History From the CIROS-1 Drillhole, McMurdo Sound*, *DSIR Bull.*, vol. 245, edited by P. Barrett, pp. 7–14, DSIR Publ., Wellington.

Wilson, D. S., and B. P. Luyendyk (2009), West Antarctic paleotopography estimated at the Eocene–Oligocene climate transition, *Geophys. Res. Lett.*, *36*, L16302, doi:10.1029/2009GL039297.

Wilson, D. S., S. S. R. Jamieson, P. J. Barrett, G. Leitchenkov, K. Gohl, and R. D. Larter (2012), Antarctic topography at the Eocene-Oligocene boundary, *Palaeogeogr. Palaeoclimatol. Palaeoecol.*, *335–336*, 24–34, doi:10.1016/j.palaeo.2011.05.028.

Wilson, T. J. (1999), Cenozoic structural segmentation of the Transantarctic rift flank in southern Victoria Land, *Global Planet. Change*, *23*, 105–127, doi:10.1016/S0921-8181(99)00053-3.

Zattin, M., F. M. Talarico, and S. Sandroni (2010), Integrated provenance and detrital thermochronology studies in the ANDRILL AND-2A drill core: Late Oligocene–early Miocene exhumation of the Transantarctic Mountains (Southern Victoria Land, Antarctica), *Terra Nova*, *22*, 361–368, doi:10.1111/j.1365-3121.2010.00958.x.